Catalysis Science & Technology

ROYAL SOCIETY OF CHEMISTRY

PAPER

View Article Online
View Journal | View Issue

Cite this: *Catal. Sci. Technol.*, 2024, **14**, 5464

Structure sensitivity of the low-temperature dehydrogenation of perhydro dibenzyltoluene on supported platinum nanoparticles†

Yazan Mahayni, [ab] Lukas Maurer, [ab] Franziska Auer,[a] Andreas Hutzler, [a] Peter Wasserscheid [ab] and Moritz Wolf *[c]

In this study, the structure sensitivity of the dehydrogenation reactions of the commonly used liquid organic hydrogen carrier (LOHC) molecules perhydro dibenzyltoluene (H18-DBT) and perhydro benzyltoluene (H12-BT) is investigated. We focus on the hydrogen release at moderate reaction temperatures, which is particularly relevant to enable heat integration of the LOHC dehydrogenation process with, for example, high-temperature fuel cells for an enhanced overall efficiency. To determine the most suitable platinum nanoparticle size with the highest surface specific productivity, a colloidal approach was used for the synthesis of Pt/Al_2O_3 catalysts with well-defined nanoparticle sizes. These catalysts were used in the dehydrogenation reactions of H18-DBT and H12-BT in the temperature ranges of 250–280 °C and 220–240 °C, respectively. A structure sensitivity was identified in both cases, which becomes particularly prominent at lower reaction temperatures. This is attributed to the overall slower reaction kinetics and the amplified differences of the adsorption strength on different surface sites. A maximum in surface specific productivity was found for catalysts with a Pt nanoparticle size of 2.6 nm for H18-DBT and 2.3 nm for H12-BT dehydrogenation. It is assumed that the observed structure sensitivity is mainly due to an optimal surface composition of the nanoparticles with an ideal balance between strongly adsorbing corner and edge sites and less active terrace sites. At low temperatures, desorption from low coordinated sites is limiting for nanoparticles below 2.3 nm, while the increasing share of terrace sites in nanoparticles larger than 2.7 nm reduces the overall productivity of the catalyst due to their lower specific activity. This behavior becomes less pronounced at higher temperatures. The dehydrogenation of H12-BT was even shown to be rather structure insensitive at 240 °C.

Received 8th January 2024,
Accepted 26th July 2024

DOI: 10.1039/d4cy00032c

rsc.li/catalysis

Introduction

The use of hydrogen as an energy carrier plays an important role for future energy distribution and supply from renewable sources. Renewable energy sources, such as solar or wind, are subject to geographical, daily, and seasonal fluctuations, which can lead to a discrepancy between energy supply and demand.[1] Hydrogen, produced by electrolysis of water with renewable electricity, can help to overcome these imbalances. Moreover, the use of hydrogen may facilitate the globalization of the renewable energy market in case of efficient long-term storage and transportation solutions.[2] Reuß *et al.* point out that hydrogen as an energy carrier has lower costs and losses when compared to high-voltage direct current transmission for transportation over distances of more than 500 km.[3]

In order to store or transport large quantities of molecular hydrogen, compression to high pressure or liquefaction at low temperature are common approaches to increase the low volumetric energy density of hydrogen under ambient conditions (3 W h L^{-1}). Both options are associated with a high energy demand and safety issues due to the handling of molecular hydrogen, while the required development of a new infrastructure for hydrogen logistics poses another challenge.[4] One possibility to overcome this is the use of alternative storage and transport media such as liquid organic hydrogen carriers (LOHCs). LOHC systems consist of hydrogen-rich and hydrogen-lean compounds which enable a reversible chemical binding of hydrogen in their molecular structure. Examples of promising LOHC pairs are dibenzyltoluene/perhydro dibenzyltoluene (H0-DBT/H18-DBT)

[a] *Forschungszentrum Jülich GmbH, Helmholtz-Institute Erlangen-Nürnberg for Renewable Energy (IEK-11), Erlangen, Germany*
[b] *Friedrich-Alexander-Universität Erlangen-Nürnberg (FAU), Lehrstuhl für Chemische Reaktionstechnik, Erlangen, Germany*
[c] *Karlsruhe Institute of Technology (KIT), Engler-Bunte-Institut & Institute of Catalysis Research and Technology, Hermann-von-Helmholtz-Platz 1, 76344 Eggenstein-Leopoldshafen, Karlsruhe, Germany. E-mail: moritz.wolf@kit.edu*
† Electronic supplementary information (ESI) available. See DOI: https://doi.org/10.1039/d4cy00032c

and benzyltoluene/perhydro benzyltoluene (H0-BT/H12-BT).[5,6] Both systems exhibit a volumetric energy density close to 2.0 kW h L^{-1}, which is higher than the value of 1.3 kW h L^{-1} for pressurized hydrogen at 700 bar.[4] Moreover, LOHCs should provide a broad liquid range, a low toxicity when compared to common fuels, a high stability to ensure circular use, and similar properties like hydrocarbon-based fuels to enable use of existing infrastructures in order to simplify implementation of the LOHC technology.[1,2,6–8] The chemical reactions of the LOHC cycle are catalytic hydrogenation and dehydrogenation through which hydrogen is either chemically bound to or released from the LOHC molecules. Both reactions require a catalyst which is typically a supported precious metal, *e.g.*, Pt on alumina (Pt/Al_2O_3).[9–11]

Recently, several options for increasing the efficiency of the LOHC concept have been discussed. A promising approach is the heat integration between the energy-intensive dehydrogenation reaction and adjacent processes, *e.g.*, coupling the dehydrogenation with the heat production from high-temperature fuel cells.[12–14] For such coupling of different processes, a lower dehydrogenation temperature than the commercially applied 300 to 340 °C facilitates heat integration and allows for higher efficiencies of the overall process.[15] In this respect, the development of a high-performance catalyst for low operation temperatures <300 °C represents a crucial step towards this goal. Therefore, the influence of a lower dehydrogenation temperature on hydrogen release from H18-DBT and H12-BT needs to be further investigated to develop optimized Pt/Al_2O_3 catalysts.

Structure sensitivity of the dehydrogenation of H18-DBT over Pt/Al_2O_3 catalysts has been reported by Auer *et al.* for a reaction temperature of 310 °C (ref. 16) and generally represents an important aspect for catalyst development. Structure sensitivity is a prominent phenomenon in heterogeneous catalysis[17–19] and based on the size-dependent composition of the catalyst surface with differently coordinated atoms, *e.g.* corner, edge, and terrace sites.[20,21] More specifically, a certain coordination of surface atoms, such as B_5 sites, may even become the major descriptor for the specific activity. These ensembles consist of a combination of step and edge sites and can exhibit beneficial catalytic properties, *e.g.*, even lower adsorption energies than terrace atoms. This is described by Foppa *et al.* for the example of CO adsorption on Ru nanoparticles.[22] Common patterns of structure sensitivity have been described by van Santen (Fig. 1).[18]

The patterns link the dependence of surface specific activity to the change in the composition and coordination of surface atoms calculated for different nanoparticle sizes (Fig. 2). This geometric effect is directly linked to specific sites, such as low-coordination or high-coordination sites, which influence chemical reactions by altering the interaction of molecules with the surface of a catalyst. Aside from geometric effects, changes in the electronic properties of nanoparticles due to their size and structure may result in electronic effects. These changes affect the energy levels

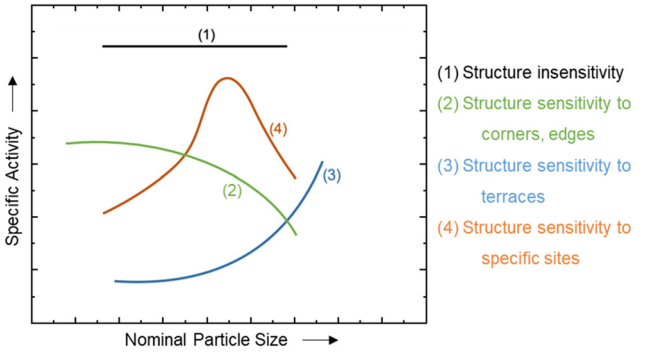

Fig. 1 Common patterns of structure-sensitive specific activities in heterogeneous catalysis (adapted from van Santen).[18]

within the nanoparticles and the electronic interactions with reactant molecules. The entanglement of both effects makes it challenging to exploit their individual contributions to catalysis effectively.[11,23,24] However, several studies directly link observed patterns of structure-sensitive specific activity to geometric effects.[16,19,25,26] Aside from structure sensitivity related to the catalyst performance, namely surface specific activity and selectivity, catalyst stability can also strongly depend on the nanoparticle size.[27–29]

For the dehydrogenation of H18-DBT using Pt catalysts, Auer *et al.* identified a broad maximum of the specific initial productivity between Pt nanoparticle sizes of 1.95 and 2.70 nm.[16] Here, the overall considered Pt nanoparticle size range was 1.2 to 4.5 nm. The elevated catalytic activity was attributed to the increased concentration of B_5 sites on the surface of the Pt nanoparticles, which theoretically peaks between 2.0 and 3.5 nm.[16,20,30]

In this work the structure sensitivity of the dehydrogenation of H18-DBT and H12-BT will be investigated at low reaction temperatures for a set of well-defined supported Pt nanoparticle sizes ranging from 1.8 to 4.0 nm. Specific activities in the dehydrogenation reaction of LOHCs are then compared to theoretical surface compositions[19] of the Pt nanoparticles to investigate geometric effects. The catalysts with narrow Pt nanoparticle size distributions were synthesized according to a previously described colloidal approach with chemical reduction and deposited on Al_2O_3.[31]

Methodology

Catalyst synthesis

The supported Pt nanoparticle catalysts were synthesized as previously reported.[31] In short, a defined amount of the capping agent polyvinylpyrrolidone (PVP, MW 40 000, Sigma Aldrich) was dissolved in 50 mL of Millipore water and ultrasonicated for 15 min to homogenize the solution. A total of 52 mg of chloroplatinic acid (H_2PtCl_6, 39 wt% Pt, Sigma Aldrich) was added to the PVP solution and the mixture was ultrasonicated for 1 min. The obtained solution was magnetically stirred at 1500 rpm and the reducing agent ($NaBH_4$, 33 mM in Millipore water, Acros Organics) was

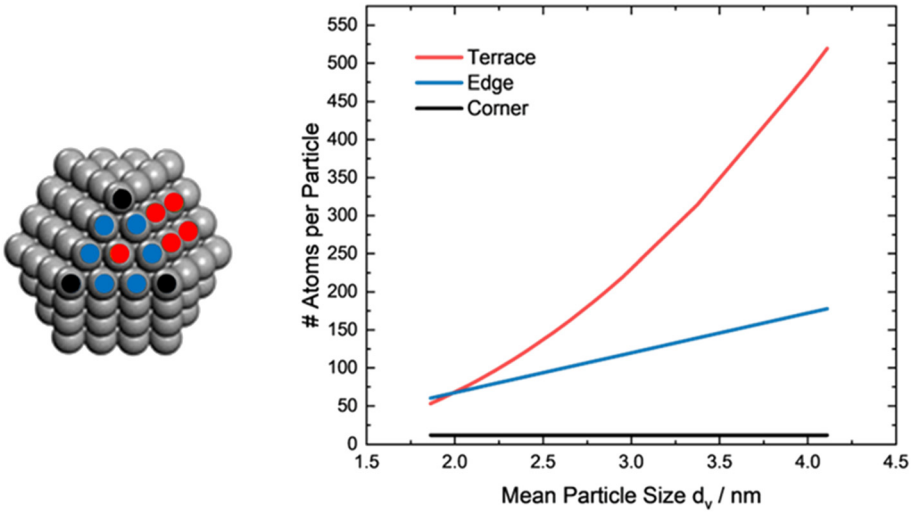

Fig. 2 Number of variously coordinated surface atoms, C_5 (corners), C_7 (edges), C_8 + C_9 (terraces), in an ideal cuboctahedral platinum particle. Calculated from Kaatz *et al.*[21]

rapidly injected. The injection of different volumes of the $NaBH_4$ solution (0.2–2.4 mL) allows for the controlled synthesis of Pt nanoparticles with certain sizes (see Table S1 in the ESI†). After 1 min of stirring, an alumina powder (PURALOX TH100/150, 35–100 μm, 150 m^2 g^{-1}, Sasol Germany) was added and the nanoparticles were immobilized overnight under moderate stirring to ensure a homogeneous distribution on the support. A loading of 0.2 wt% Pt was targeted for all catalysts with the addition of 10 g alumina support material. Solvent evaporation was carried out at 80 °C and 250 mbar in a rotary evaporator to obtain the catalyst for characterisation and catalytic testing.

Catalyst characterization

The Pt loadings of the catalysts were assessed by means of inductively coupled plasma optical emission spectroscopy (ICP-OES) using a Ciros CCD device by Spectro Analytical Instruments. The solid catalyst samples were dissolved in a concentrated $HCl:HNO_3:HF$ mixture (3 : 1 : 1 volumetric ratio) with microwave digestion. Before analysis, the instrument was calibrated with a standard solutions of Pt.

Electron microscopy was applied to analyze the size and size distribution of Pt nanoparticles. High-resolution scanning transmission electron microscopy (HRSTEM) was conducted using a Thermo Fischer Talos F200i instrument for the analysis of unsupported nanoparticles drop-casted onto carbon-coated copper grids. The software ImageJ[32] was used to evaluate the lattice distances in selected nanoparticles. Here, the contrast of the image is enhanced, followed by a fast Fourier transform bandpass filter for isolating specific frequency ranges in the image to reduce the noise and enhance lattice fringes. Then, a line is drawn across the lattice planes and a contrast profile scan is conducted and plotted. The distances between the peaks, corresponding to the lattice distances, are measured at different positions along the nanoparticle and averaged. Transmission electron microscopy (TEM) of the supported catalysts was conducted using carbon-coated copper grids and a Philips CM30 instrument. The size analysis of nanoparticles was conducted separately by two operators using ImageJ,[32] considering at least 150 Pt nanoparticles from different areas of the sample. The mean volume size (d_V) of the nanoparticles is calculated according to eqn (1).[20,33]

$$d_V\ [\mathrm{nm}] = \frac{\sum n_i \cdot d_i^4}{\sum n_i \cdot d_i^3} \quad (1)$$

The distribution of Pt nanoparticle sizes is presented by means of the volume density distribution (q_3 distribution), which is more sensitive to variously sized nanoparticles. The volume–area size (d_{VA}) is calculated according to eqn (2), while the dispersion of Pt is calculated using eqn (3).[20,33]

$$d_{VA}\ [\mathrm{nm}] = \frac{\sum n_i \cdot d_i^3}{\sum n_i \cdot d_i^2} \quad (2)$$

$$D = 6 \cdot \frac{V_{Pt}/A_{Pt}}{d_{VA}} \quad (3)$$

where V_{Pt} and A_{Pt} correspond to the volume (15.10 $Å^3$) and surface area (8.07 $Å^2$) of a Pt atom, respectively.[33]

The surface composition of the differently sized nanoparticles is approximated based on the mathematical descriptors of Kaatz *et al.*[21] (Fig. 2). In this study, we assume a structure of ideal cuboctahedron Pt nanoparticles. The approximated number of atoms in a nanoparticle is then differentiated into corners, edges, and terraces to link the proportion of these sites to observed catalyst activities. Such surface sites can only be estimated since they vary for each individual nanoparticle based on surface defects, reaction conditions, *etc.* The error associated to this approximation can be expected to be similar for all different sizes, allowing

for reasonable conclusions and hypotheses on potential structural dependencies.

Catalytic testing

Dehydrogenation experiments were conducted in a semi batch glass set-up. Certain amounts of H18-DBT or H12-BT (degree of hydrogenation >97.5%; Hydrogenious LOHC Technologies GmbH, Germany) were weighed into a 100 mL four-neck round-bottomed flask at room temperature to provide a total amount of 2 g of reversibly bound hydrogen (m(H18-DBT/H12-BT) = 32 g). A type K thermocouple, a catalyst dosing device and an argon inlet line were connected to the side necks of the flask, while an intensive condenser was attached to the middle neck. A certain amount of catalyst was loaded into the dosing device to yield a Pt : LOHC ratio of 0.1 mol%. Before the start of the experiment, an argon flow of 100 mL min^{-1} for H18-DBT or 300 mL min^{-1} for H12-BT was controlled by a mass-flow controller (Bronkhorst Deutschland Nord GmbH) to provide an oxygen-free atmosphere and to act as a carrier gas for hydrogen during dehydrogenation. The flask was then heated to the desired reaction temperature by a heating jacket in combination with a temperature controller. After reaching the reaction temperature, the catalyst in the dosing device was released into the preheated LOHC to initiate the reaction.

For quantifying the amount of released hydrogen in the dehydrogenation of H18-DBT, ^{1}H NMR spectroscopy is applied for the calculation of the degree of hydrogenation. This is defined as the molar ratio of the released hydrogen to the total maximum of reversibly bound hydrogen (DoH, eqn (4)). Here, a few drops of the liquid Hx-DBT sample are withdrawn *via* a glass pipette at the following time intervals: 0, 2.5, 5, 7.5, 10, 12.5, 15, 20, 30, 60, 90, 120 min. The samples are rinsed into an NMR analysis tube with at least 0.8 mL of deuterated chloroform. The ^{1}H NMR spectra are acquired using an ECX 400 spectrometer (JEOL) and evaluated with ACD SpecManager software (ACD Labs). This is realized through the integration of the respective signals of aromatic hydrogen atoms (in the 6.5–7.5 ppm range) and their correlation to the integral of the signals of all hydrogen atoms, *i.e.*, ratio of the respective areas. Do *et al.*[34] showcased a correlation between the degree of hydrogenation for Hx-DBT ($\mathrm{DoH_{DBT}}$) and the relative decrease in aromatic protons. The corresponding mathematical expressions according to eqn (4)–(6) assume a statistical reaction pathway for the dehydrogenation of H18-DBT. The degree of dehydrogenation ($\mathrm{DoDH_{DBT}}$) is then calculated using eqn (7).

$$\mathrm{DoH} = \frac{n_{\mathrm{H_2}}}{n_{\mathrm{total\,H_2}}} \tag{4}$$

$$x = \frac{A_{\mathrm{aromatic\,H}}}{A_{\mathrm{total\,H}}} \tag{5}$$

$$\mathrm{DoH_{DBT}} = 1.3945x^6 - 4.0937x^5 + 5.6287x^4 - 5.207x^3 + 4.0098x^2 - 2.9217x + 1 \tag{6}$$

$$\mathrm{DoDH_{DBT}} = 1 - \mathrm{DoH_{DBT}} \tag{7}$$

For the dehydrogenation of H12-BT, a thermal conductivity detector (Messkonzept GmbH, Germany) was used to analyze the gas fraction of hydrogen in the argon-rich off gas $X_{\mathrm{H_2/Ar}}$. The Pt-based productivity of the catalyst is calculated according to eqn (9) using the volumetric ratio $X_{\mathrm{H_2/Ar}}$, the applied argon flow rate $\dot{V}_{\mathrm{Ar}}$, the density of hydrogen $\rho_{\mathrm{H_2}}$ at 60 °C, the catalyst mass m_{catalyst} and the Pt loading of the catalyst w_{Pt}.

$$\mathrm{DoDH_{BT}} = \frac{n_{\mathrm{H_2}}(t)}{n_{\mathrm{total\,H_2}}} = \frac{X_{\frac{\mathrm{H_2}}{\mathrm{Ar}}}(t)\cdot\dot{V}_{\mathrm{Ar}}\cdot\rho_{\mathrm{H_2}}/M_{\mathrm{H_2}}}{n_{\mathrm{total\,H_2}}} \tag{8}$$

$$P_{\mathrm{Pt}}(t) = \frac{\Delta\mathrm{DoDH}_{\mathrm{BT/DBT}}}{m_{\mathrm{catalyst}}\cdot w_{\mathrm{Pt}}} \tag{9}$$

For a comparison of the specific activity of all dehydrogenation catalysts with different Pt nanoparticle sizes, the initial productivity ($P_{\mathrm{Pt,2–10\%}}$) between 2% and 10% degree of dehydrogenation ($\mathrm{DoDH_{BT}}$, eqn (8)) is normalized to the accessible fraction of Pt surface atoms with the help of the dispersion D. This initial surface specific productivity ($P_{\mathrm{Pt,surf}}$) is calculated according to eqn (10).

$$P_{\mathrm{Pt,surf}} = \frac{P_{\mathrm{Pt,2–10\%}}}{D} \tag{10}$$

Results

Supported Pt model catalysts were prepared according to a previous study.[31] First, a range of well-defined Pt nanoparticles with mean volumetric sizes of 1.8 to 4.0 nm were synthesized *via* a colloidal approach with chemical reduction and immobilized on an Al_2O_3 support (BET surface area: 162 m^2 g^{-1}, BJH pore size 20 nm, Fig. S1 and S2 in the ESI†). The nanoparticle sizes were determined based on TEM analysis of supported platinum nanoparticles (Fig. S3–S6†). The target loading of all catalysts was 0.2 wt% to ensure sufficient particle–particle distances after immobilization. The metal loadings were confirmed by means of ICP-OES, while a standard deviation of ±0.02 wt% was obtained (Table S1 in the ESI†).

The accessibility of the Pt surface upon chemical reduction was confirmed using CO as probe molecule, but was also demonstrated for the significantly larger H12-BT molecule.[31] Hence, the model catalysts enable studying the structure sensitivity of the low-temperature dehydrogenation of H18-DBT and H12-BT without previous exposure to elevated temperatures. The actual thermal stability of the supported Pt nanoparticles was evaluated by annealing at 250 °C under a N_2 atmosphere (see the ESI†). HRSTEM analysis before and after this exposure (Fig. S7A and B†) simulating thermal stress during catalytic application without contamination of the catalyst exhibits marginal changes of the Pt nanoparticle size distribution (Fig. S7C and D†).

Hence, thermal exposure of the model catalysts to elevated temperatures that are relevant for the herein conducted performance tests does not affect the size of well-defined supported nanoparticles. HRSTEM imaging was also conducted on unsupported Pt nanoparticles, which allowed for the analysis of the Pt lattice planes (Fig. 3). The crystallographic (100) and (111) facets with lattice distances of 0.392 and 0.226 nm, respectively,[35] were identified. These are common in cuboctahedron nanoparticles.

Structure sensitivity of the dehydrogenation of perhydro dibenzyltoluene (H18-DBT)

Based on the previous results on the structure sensitivity of the dehydrogenation of H18-DBT at 310 °C,[16] catalysts with Pt nanoparticle sizes in the range of 2.0 to 4.0 nm were tested at lower reaction temperatures of 280 and 250 °C. The selected range of volumetric nanoparticle sizes covers the reported range with maximum initial surface specific productivity, which was previously linked to the high proportion of B_5 sites.[16] The herein obtained results at lower operation temperatures are compared with the data of Auer *et al.* previously obtained at 310 °C (Fig. 4).[16] The performance of each catalyst during these semi batch dehydrogenation experiments is described in the ESI† (Table S2). It becomes evident that the structure sensitivity is significantly amplified at lower reaction temperatures.

At 250 °C, the highest initial surface specific productivity of 0.60 g_{H_2} $g_{Pt,surf}^{-1}$ min^{-1} was observed for a catalyst with a Pt nanoparticle size of 2.6 nm, whereas the catalyst with the smallest size of 2.0 nm showed an initial productivity of 0.17 g_{H_2} $g_{Pt,surf}^{-1}$ min^{-1}. For larger nanoparticles, the initial productivity was below 0.10 g_{H_2} $g_{Pt,surf}^{-1}$ min^{-1} for a mean Pt nanoparticle size of 3.4 nm. This corresponds to a more than sixfold increase of the initial productivity at 250 °C within the considered size range. At 280 °C, the dehydrogenation of H18-DBT and the specific initial productivity of the dehydrogenation catalysts become less sensitive to the Pt nanoparticle size than at the lowest temperature (Fig. 2). An initial productivity of 1.27 g_{H_2} $g_{Pt,surf}^{-1}$ min^{-1} was obtained for the catalysts with mean volumetric sizes below 2.3 nm, while a productivity increase to 1.71 g_{H_2} $g_{Pt,surf}^{-1}$ min^{-1} was observed for the catalyst with 2.6 nm Pt nanoparticles. For sizes larger than 2.8 nm, the specific productivity declined to a lower level comparable to the smallest sizes. A minimum productivity of 1.18 g_{H_2} $g_{Pt,surf}^{-1}$ min^{-1} was observed for the largest studied size of 4.0 nm. The significance of the slightly increased maximum initial productivity at a Pt nanoparticle size of 2.6 nm has been confirmed by three reproductions. Comparison of these results with the available data for the

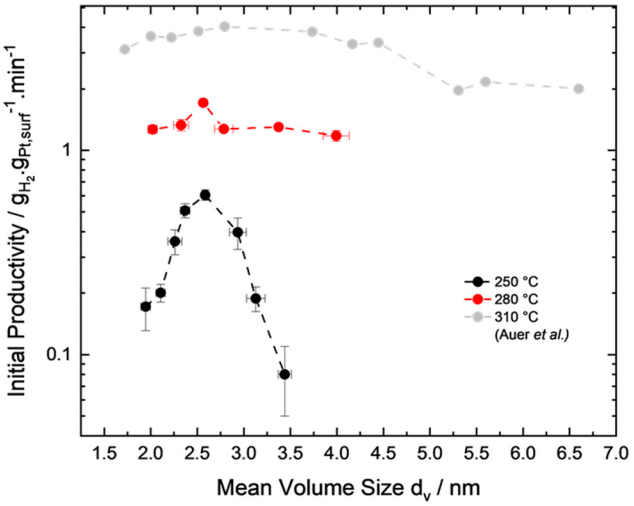

Fig. 4 Initial surface specific productivity of Pt/Al_2O_3 catalysts with defined Pt nanoparticle sizes in the dehydrogenation of H18-DBT at different reaction temperatures. Reaction conditions: T = 250 °C (black); 280 °C (red), $n_{Pt}:n_{LOHC}$ = 0.1 mol%, F_{Ar} = 100 mL min^{-1}, $t_{Reaction}$ = 120 min, catalyst loading = 0.2 wt% Pt. Synthesis conditions: surfactant : Pt precursor ratio = 5 g_{PVP} g_{Pt}^{-1}, reducing agent : Pt precursor ratio = 0.2–0.4 mol_{NaBH_4} mol_{Pt}^{-1}. Grey data points adapted from Auer *et al.*[16] Reaction conditions: T = 310 °C (grey), $n_{Pt}:n_{LOHC}$ = 0.1 mol%, F_{Ar} = 0 mL min^{-1}, $t_{Reaction}$ = 120 min, catalyst loading = 0.3 wt% Pt. Error bars represent the standard deviation of the initial productivity from three reproductions and of the mean size. Dashed lines to guide the eye.

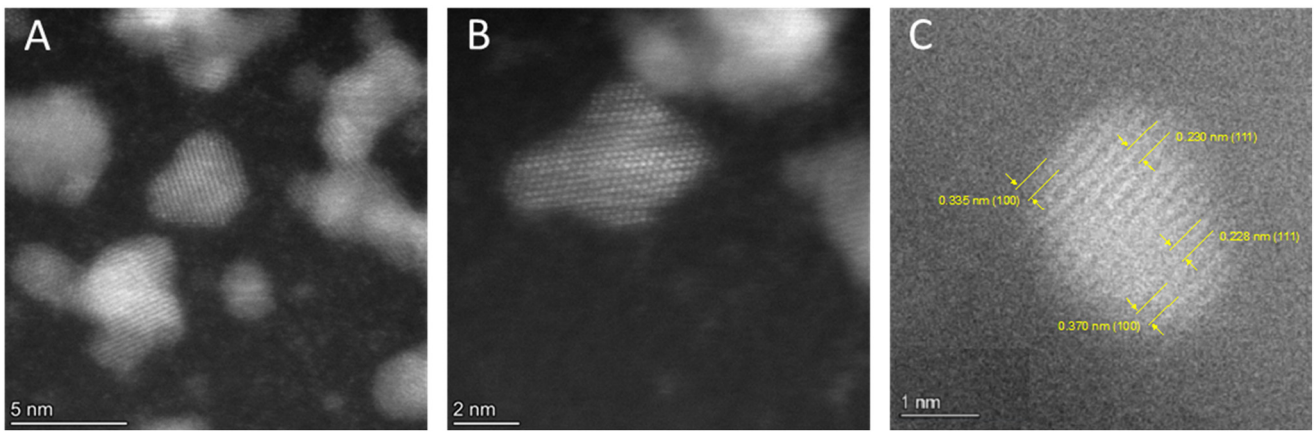

Fig. 3 HRSTEM of unsupported Pt nanoparticles of (A) 4.5, (B) 6.0, and (C) 2.6 nm synthesized *via* aqueous $NaBH_4$ solutions with identified (100) and (111) facets.

dehydrogenation of H18-DBT at 310 °C (ref. 16) reveals a less pronounced structure sensitivity at increased operation temperatures. This may stem from the lower equilibrium conversion and the generally slower reaction kinetics for the dehydrogenation reaction at lower reaction temperatures, which may amplify miniscule differences in the intrinsic activity of differently coordinated surface atoms.

Structure sensitivity of the dehydrogenation of perhydro benzyltoluene (H12-BT)

Following the same approach, the structure sensitivity of the dehydrogenation of H12-BT was investigated. A temperature range of 220 to 240 °C was selected for these experiments, while 0.2 wt% Pt/Al_2O_3 model catalysts with mean volumetric Pt nanoparticle sizes in the range of 1.8 to 4.0 nm were used. The initial productivities of the catalysts were, once again, normalized to the Pt surface atoms (Fig. 5), while the individual semi batch tests are shown in the ESI† (Table S3). The observed correlations between Pt nanoparticle size and surface specific catalyst activity clearly point towards a structure sensitivity of the dehydrogenation of H12-BT within the investigated temperature range.

Expectedly, the structure sensitivity is the least pronounced at the highest reaction temperature of 240 °C. Interestingly and regardless of their higher proportion of terrace sites with an expected lower intrinsic activity,[16] catalysts with Pt nanoparticle sizes >2.7 nm exhibited a plateau with the highest specific initial productivities of 0.72 g_{H_2} $g_{Pt,surf}^{-1}$ min^{-1}. Similar to the observations for the dehydrogenation of H18-DBT, this indicates that the reaction kinetics at temperatures ≥240 °C are sufficiently fast to obtain such improved activities regardless of the nature of surface atoms and composition of nanoparticles. In contrast, the structure sensitivity at dehydrogenation temperatures of 220 and 230 °C is more pronounced with maximum initial productivities of 0.19 and 0.40 g_{H_2} $g_{Pt,surf}^{-1}$ min^{-1}, respectively, for a Pt nanoparticle size of 2.3 nm. This size provides an intermediate share of low coordinated edge atoms and a surface composition suitable to form B_5 sites.[21,36] In particular, the number of edge atoms is of great importance for the formation of B_5 sites.[37]

To demonstrate the absence of mass transport limitations in all experiments, an Arrhenius plot was exemplarily determined for the dehydrogenation of H12-BT using the catalyst with an optimum Pt nanoparticle size of 2.3 nm (Fig. S8†). Minimum mass transport limitations are expected due to the selection of a catalyst support material with a mean pore size of 22 nm in combination with the use of fine powder (particle size <100 μm).[38] An activation energy of 182 ± 8 kJ mol^{-1} was derived from the Arrhenius plot, which lies within the expected range[11] and is significantly higher than values determined for other LOHC systems in the pore diffusion limited regime and therefore suggests that the role of the mass transport may be neglected in our study.[39]

Finally, continuous dehydrogenation of H12-BT was conducted in a fixed-bed lab reactor at 250 °C to demonstrate the suitability of the herein studied catalysts (see the ESI†). For application in a fixed-bed reactor, 2.3 nm sized Pt nanoparticles were immobilized on spherical Al_2O_3 pellets instead of Al_2O_3 powder, which was used in semi-batch testing. At 250 °C, the 0.18 wt% Pt/Al_2O_3 catalysts maintained a steady productivity of approx. 0.5 g_{H_2} $g_{Pt,surf}^{-1}$ min^{-1} at a DoDH of 5% (Fig. S9†), which is comparable to semi-batch results (Fig. 5) and to the performance of industrial catalysts.[14] No side product formation was observed, while minor quantities of fluorene species were observed at increased DoDH during semi-batch dehydrogenation at 250 °C (Fig. S10†).

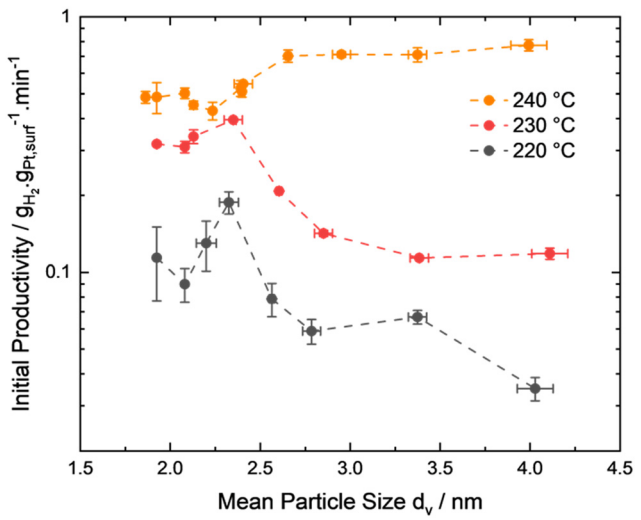

Fig. 5 Initial surface specific productivity of Pt/Al_2O_3 catalysts with defined Pt nanoparticle sizes in the dehydrogenation of H12-BT at different reaction temperatures. Reaction conditions: T = 220 °C (black), 230 °C (red), 240 °C (orange); $n_{Pt}:n_{LOHC}$ = 0.1 mol%, F_{Ar} = 300 mL min^{-1}, $t_{Reaction}$ = 120 min, catalyst loading = 0.2 wt% Pt. Synthesis conditions: surfactant : Pt precursor ratio = 5 g_{PVP} g_{Pt}^{-1}, reducing agent : Pt precursor ratio = 0.2–0.4 mol_{NaBH_4} mol_{Pt}^{-1}. Error bars represent the standard deviation of the initial productivity of three reproductions and the mean size. Dashed lines are guides to the eye.

Discussion

The observed structure sensitivity of the dehydrogenation of perhydro dibenzyltoluene over Pt/Al_2O_3 catalysts features transitions between common structure sensitivity patterns (Fig. 1) for the different temperatures. This results in a pronounced dependence on the surface composition of differently sized Pt nanoparticles (Fig. 2) and vast differences in the specific kinetic limitations for different active sites, *e.g.*, corners, edges, terraces. Here, the conversion of intermediates on the surface and particularly the desorption of aromatic products are expected to induce the distinct structure sensitivity, which becomes most evident at low temperatures. The desorption of (partially) dehydrogenated aromatic species is assumed to be the rate-limiting step during dehydrogenation.[40–42] Sinfelt *et al.* identified the

desorption of toluene as the rate-determining step during dehydrogenation of methylcyclohexane on Pt-based catalysts.[43] The adsorption strength of aromatic species on the surface of noble metals was found to be generally higher than that of their aliphatic counterparts.[42,44–47] Consequently, (partially) dehydrogenated aromatic species are expected to undergo a stronger adsorption on the active sites of the catalyst when compared to the hydrogenated LOHC molecules. As the strength of the molecular interaction with the active sites depends not only on the nature of the molecule, *i.e.*, aromatic or aliphatic, but also on the quality and quantity of involved surface atoms, the structure and nanoparticle size of the supported catalyst play an important role. At lower reaction temperatures, the energy barrier for product desorption is more difficult to overcome and the different adsorption strengths of active Pt sites become more evident. The resulting amplified structure sensitivity is then a result of a drastically decelerated kinetics on Pt nanoparticles at low reaction temperatures, which can only be overcome by optimum surface composition for a certain nanoparticle size. DFT simulations by Moro Ouma *et al.*[42] on the adsorption of H18-DBT on different active sites support this hypothesis. The group examined the adsorption behavior of various isomers on ideal cuboctahedral Pt nanoparticles. The adsorption energy on different surface atoms strongly depends on their coordination and contributes to the electronic effects of structure sensitivity. A strong adsorption of H18-DBT was reported on low coordinated corner and edge atoms (adsorption energies 190–278 kJ mol^{-1}), while a weaker adsorption was found for higher coordinated terrace atoms (150–166 kJ mol^{-1}).

Certain similarities may be identified for both LOHC systems for the studied temperature ranges (Fig. 4 and 5). The dehydrogenation of H12-BT only deviates from that of H18-DBT at the highest studied temperature of 240 °C, at which the largest Pt nanoparticle sizes outperform the smaller ones, potentially because the reaction becomes structure insensitive at higher temperatures. This may also be the case for the dehydrogenation of H18-DBT at temperatures exceeding 310 °C. The major causes of limitation, resulting in a structure-sensitive dehydrogenation, can be generalized for small nanoparticle sizes below 2.3 nm, an optimum size range of 2.3 to 2.7 nm, and larger nanoparticles (Fig. 6). The combination of low dehydrogenation temperatures (H18-DBT: 250 °C; H12-BT: 220–230 °C) and small nanoparticle sizes (<2.3 nm) results in a low activity due to the high adsorption energy of the (partially) dehydrogenated LOHC species on the exposed active sites. At a reaction temperature of 280 °C for H18-DBT and 240 °C for H12-BT, no such desorption limitation is observed. In turn, less pronounced structure dependencies occur for both LOHCs.

A certain range of nanoparticle sizes (2.3–2.7 nm) leads to improved activities for both LOHC molecules, which can be linked to optimum surface compositions for an efficient dehydrogenation reaction (Fig. 6). This size range provides the ideal ratio between corner and edge atoms. To illustrate this size-dependent change in surface composition, the proportion of different types of surface atoms, *i.e.*, corners, edges and terraces, for the size range considered in this work is calculated using mathematical models for an ideal cuboctahedral nanoparticle (Fig. 2).[20,21,36] For Pt nanoparticles with a mean volumetric size of 2.0 nm, low coordinated corner and edge atoms represent more than 51% of all surface atoms.[21,36,42] This surface composition is also suitable to form a high fraction of B_5 sites which can be an example for highly efficient surface structures for LOHC dehydrogenation. When comparing the optimum Pt nanoparticle sizes for both H12-BT and H18-DBT dehydrogenation, a smaller value (2.3 nm) was identified for H12-BT than for H18-DBT (2.6 nm). This

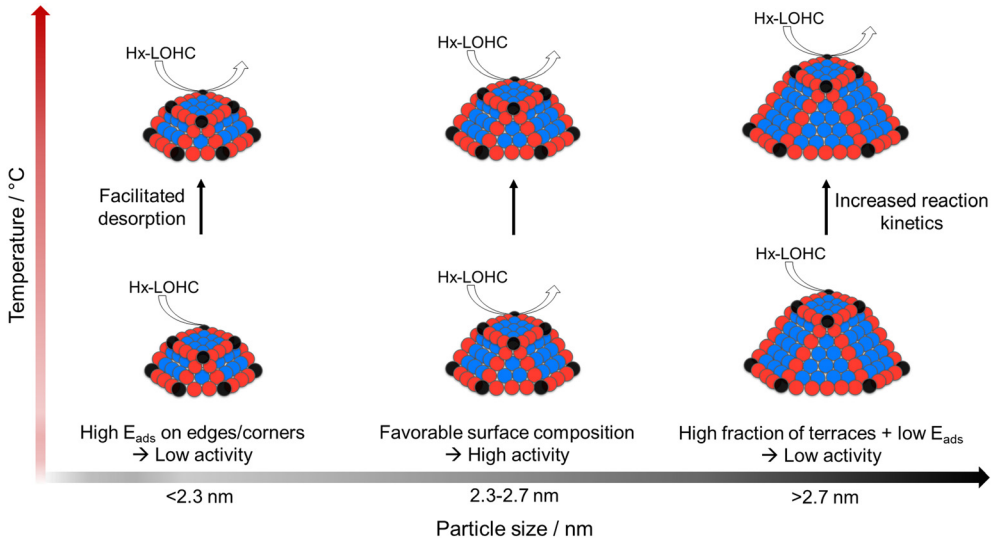

Fig. 6 Proposed origin of the low-temperature structure sensitivity of the dehydrogenation of H18-DBT or H12-DBT using Pt depending on the nanoparticle size range.

observation is possibly related to the smaller size of the H*x*-BT molecule (~1 nm), whereas H*x*-DBT exhibits an approximate size of 1.4 nm.[48]

For large Pt particle sizes (>2.7 nm), the relative contribution of terrace atoms at the surface increases (Fig. 2).[21] Hence, the intrinsic activity of a large fraction of surface atoms is reduced, which restricts the overall dehydrogenation rate at low reaction temperatures (H18-DBT: 250 °C; H12-BT: 220–230 °C). Expectedly, increasing the temperature enhances the kinetics of the dehydrogenation at terrace sites (Fig. 6). For the dehydrogenation of H12-BT, slightly higher activities are observed for large nanoparticles at the highest temperature of 240 °C. This points towards a structure insensitivity of the dehydrogenation at even higher temperatures.

The identified structure dependence illustrates one important aspect in catalyst development for hydrogen release from LOHC systems, which aims for maximum H_2 release and a selectivity of ideally 100%. For operation at low temperatures, optimization of the Pt nanoparticle size is inevitable to overcome the identified kinetic limitations for the different size regimes (Fig. 6). While operation at elevated temperatures may suppress such limitations, the high intrinsic activity of low coordinated Pt atoms may cause the formation of fluorene derivatives as side products of a consecutive "deep" dehydrogenation of H0-LOHC.[5,49,50] Hence, the optimum operation temperature window for technical LOHC dehydrogenation is limited on the lower end by slow and structure-sensitive kinetics and at the higher end by enhanced formation of side products. To suppress the latter, selective poisoning of the Pt surface by sulphur has been successfully demonstrated but is also detrimental to the overall activity of the catalyst.[51–53] In consequence, a combination of large Pt nanoparticles with a large contribution of terrace sites, selective poisoning of the low coordinated atoms, and high operation temperatures currently represents the best technical solution but leaves room for further developments targeting enhanced Pt-based productivity.

Summary and conclusions

In this study, the structure sensitivity of the dehydrogenation of the LOHC molecules H18-DBT and H12-BT was investigated for different reaction temperatures. For the dehydrogenation of H18-DBT, experiments at 280 and 250 °C were carried out and compared to previous investigations at 310 °C. For H12-BT, the temperature range between 220 and 240 °C was considered. It was shown that the structure sensitivity is amplified at lower temperatures in both cases. For H18-DBT, a maximum of the specific, initial productivity was found at a mean volumetric Pt nanoparticle diameter of 2.6 nm, while a diameter of 2.3 nm proved best for H12-BT. The difference in the optimal Pt particle size is probably due to the different molecular dimensions of H*x*-DBT and H*x*-BT. At the lowest reaction temperature considered, the initial surface specific productivity for a catalyst with the optimum Pt nanoparticle size is 3.5 and 1.9 times higher for H18-DBT and H12-BT, respectively, compared to a catalyst with 2.0 nm Pt nanoparticles. Overall, the structure-sensitive nature of the dehydrogenation reactions at these temperatures was attributed to different desorption properties and a site-specific intrinsic activity, which results in a variety of kinetic limitations. Larger nanoparticles provide a smaller fraction of low coordinated surface atoms, which are associated with strong adsorption energies, particularly of the aromatic intermediates and products. Hence, the lower share of such sites in large nanoparticles facilitates the desorption of the aromatic dehydrogenation products. However, a low activity is observed for low temperatures due to the lower intrinsic activity of such terrace sites. At the optimal size, the nanoparticles exhibit an intermediate proportion of edge atoms and a suitable composition for the formation of active B_5 sites. Taking these findings into account, the efficiency of catalysts for low-temperature LOHC dehydrogenation processes can be drastically improved as shown in this contribution.

Data availability

All relevant data are available from the authors upon request. Please contact the corresponding author.

Conflicts of interest

Peter Wasserscheid is co-founder and minority shareholder of Hydrogenious LOHC Technologies GmbH, Erlangen, a company that has commercialised equipment for hydrogen storage using the LOHC technology.

Acknowledgements

Financial support by the Bavarian Ministry of Economic Affairs, Regional Development and Energy through the project "Emissionsfreier und stark emissionsreduzierter Bahnverkehr auf nicht-elektrifizierten Strecken" and by the Helmholtz Research Program "Materials and Technologies for the Energy Transition (MTET), Topic 3: Chemical Energy Carriers" is highly acknowledged. Infrastructural support by DFG *via* its SFB 1452 (Catalysis at Liquid Interfaces, CLINT) is also gratefully acknowledged.

References

1 D. Teichmann, W. Arlt and P. Wasserscheid, Liquid Organic Hydrogen Carriers as an efficient vector for the transport and storage of renewable energy, *Int. J. Hydrogen Energy*, 2012, **37**, 18118.
2 D. Teichmann, W. Arlt, P. Wasserscheid and R. Freymann, A future energy supply based on Liquid Organic Hydrogen Carriers (LOHC), *Energy Environ. Sci.*, 2011, **4**, 2767.
3 M. Reuß, T. Grube, M. Robinius, P. Preuster, P. Wasserscheid and D. Stolten, Seasonal storage and alternative carriers: A flexible hydrogen supply chain model, *Appl. Energy*, 2017, **200**, 290.

4 P. Preuster, A. Alekseev and P. Wasserscheid, Hydrogen Storage Technologies for Future Energy Systems, *Annu. Rev. Chem. Biomol. Eng.*, 2017, **8**, 445.
5 T. Rüde, S. Dürr, P. Preuster, M. Wolf and P. Wasserscheid, Benzyltoluene/perhydro benzyltoluene–pushing the performance limits of pure hydrocarbon liquid organic hydrogen carrier (LOHC) systems, *Sustainable Energy Fuels*, 2022, **6**, 1541.
6 E. Herzinger and M. Wolf, Perspectives and Potential of Liquid Organic Hydrogen Carriers in the German Energy Scenario, *Chem. Ing. Tech.*, 2024, **96**, 65.
7 S. Singh, S. Jain, V. Ps, A. K. Tiwari, M. R. Nouni, J. K. Pandey and S. Goel, Hydrogen: A sustainable fuel for future of the transport sector, *Renewable Sustainable Energy Rev.*, 2015, **51**, 623.
8 N. Brückner, K. Obesser, A. Bösmann, D. Teichmann, W. Arlt, J. Dungs and P. Wasserscheid, Evaluation of industrially applied heat-transfer fluids as liquid organic hydrogen carrier systems, *ChemSusChem*, 2014, **7**, 229.
9 P. Preuster, C. Papp and P. Wasserscheid, Liquid Organic Hydrogen Carriers (LOHCs): Toward a Hydrogen-free Hydrogen Economy, *Acc. Chem. Res.*, 2017, **50**, 74.
10 J. Oh, Y. Jo, T. W. Kim, H. B. Bathula, S. Yang, J. H. Baik and Y.-W. Suh, Highly efficient and robust Pt ensembles on mesoporous alumina for reversible H_2 charge and release of commercial benzyltoluene molecules, *Appl. Catal., B*, 2022, **305**, 121061.
11 D. Strauch, P. Weiner, B. B. Sarma, A. Körner, E. Herzinger, P. Wolf, A. Zimina, A. Hutzler, D. E. Doronkin, J.-D. Grunwaldt, P. Wasserscheid and M. Wolf, Bimetallic platinum rhenium catalyst for efficient low temperature dehydrogenation of perhydro benzyltoluene, *Catal. Sci. Technol.*, 2024, **14**, 1775.
12 P. Preuster, Q. Fang, R. Peters, R. Deja, N. van Nguyen, L. Blum, D. Stolten and P. Wasserscheid, Solid oxide fuel cell operating on liquid organic hydrogen carrier-based hydrogen – making full use of heat integration potentials, *Int. J. Hydrogen Energy*, 2018, **43**, 1758.
13 G. Sievi, D. Geburtig, T. Skeledzic, A. Bösmann, P. Preuster, O. Brummel, F. Waidhas, M. A. Montero, P. Khanipour, I. Katsounaros, J. Libuda, K. J. J. Mayrhofer and P. Wasserscheid, Towards an efficient liquid organic hydrogen carrier fuel cell concept, *Energy Environ. Sci.*, 2019, **12**, 2305.
14 T. Rüde, Y. Lu, L. Anschütz, M. Blasius, M. Wolf, P. Preuster, P. Wasserscheid and M. Geißelbrecht, Performance of Continuous Hydrogen Production from Perhydro Benzyltoluene by Catalytic Distillation and Heat Integration Concepts with a Fuel Cell, *Energy Technol.*, 2023, **11**, 2201366.
15 J. Geiling, L. Wagner, F. Auer, F. Ortner, A. Nuß, R. Seyfried, F. Stammberger, M. Steinberger, A. Bösmann, R. Öchsner, P. Wasserscheid, K. Graichen, M. März and P. Preuster, Operational experience with a liquid organic hydrogen carrier (LOHC) system for bidirectional storage of electrical energy over 725 h, *J. Energy Storage*, 2023, **72**, 108478.
16 F. Auer, A. Hupfer, A. Bösmann, N. Szesni and P. Wasserscheidpeter, Influence of the nanoparticle size on hydrogen release and side product formation in liquid organic hydrogen carrier systems with supported platinum catalysts, *Catal. Sci. Technol.*, 2020, **10**, 6669.
17 M. Che and C. O. Bennett, The influence of particle size on the catalytic properties of supported metals, *Adv. Catal.*, 1989, **36**, 55.
18 R. A. van Santen, Complementary structure sensitive and insensitive catalytic relationships, *Acc. Chem. Res.*, 2009, **42**, 57.
19 C. Vogt, F. Meirer, M. Monai, E. Groeneveld, D. Ferri, R. A. van Santen, M. Nachtegaal, R. R. Unocic, A. I. Frenkel and B. M. Weckhuysen, Dynamic restructuring of supported metal nanoparticles and its implications for structure insensitive catalysis, *Nat. Commun.*, 2021, **12**, 7096.
20 R. van Hardeveld and F. Hartog, The statistics of surface atoms and surface sites on metal crystals, *Surf. Sci.*, 1969, **15**, 189.
21 F. H. Kaatz and A. Bultheel, Magic Mathematical Relationships for Nanoclusters, *Nanoscale Res. Lett.*, 2019, **14**, 150.
22 L. Foppa, C. Copéret and A. Comas-Vives, Increased Back-Bonding Explains Step-Edge Reactivity and Particle Size Effect for CO Activation on Ru Nanoparticles, *J. Am. Chem. Soc.*, 2016, **138**, 16655.
23 W. Chen, J. Ji, X. Feng, X. Duan, G. Qian, P. Li, X. Zhou, D. Chen and W. Yuan, Mechanistic Insight into Size-Dependent Activity and Durability in Pt/CNT Catalyzed Hydrolytic Dehydrogenation of Ammonia Borane, *J. Am. Chem. Soc.*, 2014, **136**, 16736.
24 H. Wang, X.-K. Gu, X. Zheng, H. Pan, J. Zhu, S. Chen, L. Cao, W.-X. Li and J. Lu, Disentangling the size-dependent geometric and electronic effects of palladium nanocatalysts beyond selectivity, *Sci. Adv.*, 2019, **5**, eaat6413.
25 N. Fischer, E. van Steen and M. Claeys, Structure sensitivity of the Fischer–Tropsch activity and selectivity on alumina supported cobalt catalysts, *J. Catal.*, 2013, **299**, 67.
26 W. Fu, W. Chen, G. Qian, W. de Chen, X. Zhou Yuan and X. Duan, Kinetics-assisted discrimination of active sites in Ru catalyzed hydrolytic dehydrogenation of ammonia borane, *React. Chem. Eng.*, 2019, **4**, 316.
27 E. Iglesia, Design, synthesis, and use of cobalt-based Fischer-Tropsch synthesis catalysts, *Appl. Catal., A*, 1997, **161**, 59.
28 M. Wolf, H. Kotzé, N. Fischer and M. Claeys, Size dependent stability of cobalt nanoparticles on silica under high conversion Fischer–Tropsch environment, *Faraday Discuss.*, 2017, **197**, 243.
29 M. Wolf, Thermodynamic assessment of the stability of bulk and nanoparticulate cobalt and nickel during dry and steam reforming of methane, *RSC Adv.*, 2021, **11**, 18187.
30 D. Astruc, in *Nanoparticles and catalysis*, ed. D. Astruc, Wiley-VCH, Weinheim, 2008, pp. 1–48.
31 Y. Mahayni, L. Maurer, I. Baumeister, F. Auer, P. Wasserscheid and M. Wolf, Batch and continuous synthesis of well-defined Pt/Al2O3 catalysts for the dehydrogenation of homocyclic LOHCs, *ChemRxiv*, 2024, preprint, DOI: **10.26434/chemrxiv-2024-slhhv**.

32 J. Schindelin, C. T. Rueden, M. C. Hiner and K. W. Eliceiri, The ImageJ ecosystem: An open platform for biomedical image analysis, *Mol. Reprod. Dev.*, 2015, **82**, 518.
33 G. Bergeret and P. Gallezot, in *Handbook of Heterogeneous Catalysis*, ed. G. Ertl, H. Knözinger, F. Schüth and J. Weitkamp, Wiley, 2008, pp. 738–765.
34 G. Do, P. Preuster, R. Aslam, A. Bösmann, K. Müller, W. Arlt and P. Wasserscheid, Hydrogenation of the liquid organic hydrogen carrier compound dibenzyltoluene – reaction pathway determination by ^{1}H NMR spectroscopy, *React. Chem. Eng.*, 2016, **1**, 313.
35 R. W. G. Wyckoff, *Crystal Structures - Volume 1*, Interscience Publishers, New York, 2nd edn, 1963.
36 A. Le Valant, C. Comminges, F. Can, K. Thomas, M. Houalla and F. Epron, Platinum Supported Catalysts: Predictive CO and H_2 Chemisorption by a Statistical Cuboctahedron Cluster Model, *J. Phys. Chem. C*, 2016, **120**, 26374.
37 J. Zhang, H. Xu and W. Li, Kinetic study of NH_3 decomposition over Ni nanoparticles: The role of La promoter, structure sensitivity and compensation effect, *Appl. Catal., A*, 2005, **296**, 257.
38 F. Auer, *PhD thesis*, Friedrich-Alexander-Universität Erlangen-Nürnberg, Erlangen, 2020, **https://open.fau.de/handle/openfau/14054**.
39 W. Peters, A. Seidel, S. Herzog, A. Bösmann, W. Schwieger and P. Wasserscheid, Macrokinetic effects in perhydro-N-ethylcarbazole dehydrogenation and H_2 productivity optimization by using egg-shell catalysts, *Energy Environ. Sci.*, 2015, **8**, 3013.
40 G. A. Somorjai and Y. Li, *Introduction to surface chemistry and catalysis*, Wiley, Hoboken, New Jersey, 2010.
41 S. Dürr, S. Zilm, M. Geißelbrecht, K. Müller, P. Preuster, A. Bösmann and P. Wasserscheid, Experimental determination of the hydrogenation/dehydrogenation-Equilibrium of the LOHC system H0/H18-dibenzyltoluene, *Int. J. Hydrogen Energy*, 2021, **46**, 32583.
42 C. N. Moro Ouma, P. Modisha and D. Bessarabov, Insight into the adsorption of a liquid organic hydrogen carrier, perhydro-i-dibenzyltoluene (i = m, o, p), on Pt, Pd and PtPd planar surfaces, *RSC Adv.*, 2018, **8**, 31895.
43 J. H. Sinfelt, H. Hurwitz and R. A. Shulman, Kinetics of Methylcyclohexane Dehydrogenation over Pt-Al_2O_3, *J. Phys. Chem.*, 1960, **64**, 1559.
44 S. J. Jenkins, Aromatic adsorption on metals via first-principles density functional theory, *Proc. R. Soc. A*, 2009, **465**, 2949.
45 C. Morin, D. Simon and P. Sautet, Trends in the Chemisorption of Aromatic Molecules on a Pt(111) Surface: Benzene, Naphthalene, and Anthracene from First Principles Calculations, *J. Phys. Chem. B*, 2004, **108**, 12084.
46 C. Morin, D. Simon and P. Sautet, Chemisorption of Benzene on Pt(111), Pd(111), and Rh(111) Metal Surfaces: A Structural and Vibrational Comparison from First Principles, *J. Phys. Chem. B*, 2004, **108**, 5653.
47 M. Saeys, M.-F. Reyniers, G. B. Marin and M. Neurock, Density Functional Study of Benzene Adsorption on Pt(111), *J. Phys. Chem. B*, 2002, **106**, 7489.
48 D. Zakgeym, T. Engl, Y. Mahayni, K. Müller, M. Wolf and P. Wasserscheid, Development of an efficient Pt/SiO_2 catalyst for the transfer hydrogenation from perhydro-dibenzyltoluene to acetone, *Appl. Catal., A*, 2022, **639**, 118644.
49 P. Modisha and D. Bessarabov, Stress tolerance assessment of dibenzyltoluene-based liquid organic hydrogen carriers, *Sustainable Energy Fuels*, 2020, **4**, 4662.
50 T. W. Kim, Y. Jo, K. Jeong, H. Yook, J. W. Han, J. H. Jang, G. B. Han, J. H. Park and Y.-W. Suh, Tuning the isomer composition is a key to overcome the performance limits of commercial benzyltoluene as liquid organic hydrogen carrier, *J. Energy Storage*, 2023, **60**, 106676.
51 F. Auer, D. Blaumeiser, T. Bauer, A. Bösmann, N. Szesni, J. Libuda and P. Wasserscheid, Boosting the activity of hydrogen release from liquid organic hydrogen carrier systems by sulfur-additives to Pt on alumina catalysts, *Catal. Sci. Technol.*, 2019, **9**, 3537.
52 X. Chen, C. H. Gierlich, S. Schötz, D. Blaumeiser, T. Bauer, J. Libuda and R. Palkovits, Hydrogen Production Based on Liquid Organic Hydrogen Carriers through Sulfur Doped Platinum Catalysts Supported on TiO_2, *ACS Sustainable Chem. Eng.*, 2021, **9**, 6561.
53 Y. Jo, T. Wan Kim, J. Oh, D. Kim and Y.-W. Suh, Mesoporous sulfur-decorated Pt–Al2O3 for dehydrogenation of perhydro benzyltoluenes: Activity-favorable adsorption of reaction species onto electron-deficient Pt atoms, *J. Catal.*, 2022, **413**, 127.